Cement and Concrete Composites 114 (2020) 103614

Contents lists available at ScienceDirect

Cement and Concrete Composites

journal homepage: http://www.elsevier.com/locate/cemconcomp

External sulphate attack of sprayed mortars with sulphate-resisting cement: Influence of accelerator and age of exposition

C. Herrera-Mesen [a,*], R.P. Salvador [b], T. Ikumi [a], S.H.P. Cavalaro [c,**], A. Aguado [a]

[a] Department of Civil and Environmental Engineering, Barcelona Tech, Polytechnic University of Catalonia, UPC, Jordi Girona 1-3, 08034, Barcelona, Spain
[b] Department of Civil Engineering, São Judas Tadeu University, 546 Taquari St., 03166-000, São Paulo, Brazil
[c] School of Architecture, Building and Civil Engineering, Loughborough University, Leicestershire, LE11 3TU, UK

ARTICLE INFO

Keywords:
Durability
External sulphate attack
Accelerators
Sprayed materials
Sulphate-resisting cement

ABSTRACT

This work evaluates the influence of the accelerator type, the cement type and age of exposure on the degradation mechanism and the durability of sprayed mortars subjected to external sulphate attack (ESA). Cores and prisms were extracted from panels sprayed with 8 mortar compositions (with 2 sulphate-resisting cement types and 4 setting accelerators) and then exposed to a sulphate solution at the ages of 7 or 28 days for 400 days. The evolution of the ESA was assessed through XRD, SEM, compressive strength, dimensional variation and ultrasonic pulse velocity. Results show that alkaline accelerators increase drastically the vulnerability of the matrix to the ESA. The degradation is enhanced by the higher solubility of aluminate phases and the increased formation of expansive phases. Results reveal that the use of sulphate-resisting cement might not suffice to mitigate severe material degradation.

1. Introduction

Recent developments in set accelerators and spraying equipment have prompted the use of sprayed mixes with Portland cement in underground and other ground contention applications. The construction process consists of spraying a cementitious mix that consolidates upon reaching the substrate [1]. The mix must have adequate consistency and setting time to enable the build-up of layers with the desired thicknesses. Accelerators work to reduce the setting times and increase the early strength of the matrix, thus enabling the faster layer deposition and execution of challenging overhead elements. The accelerators also alter the matrix short- and long-term hydration, microstructure and properties [2–4].

Immediately after spraying, the material remains in direct contact with the surrounding soil and underground water, which may contain aggressive agents such as sulphates. As they penetrate through the interconnected porous network, sulphates can react with different compounds of the cementitious matrix to form expansive phases (such as secondary ettringite and gypsum) and deteriorate the mechanical properties of the matrix in a process known as external sulphate attack (ESA). Different damage mechanisms are associated with this phenomenon. The most common one attributes the damage developed to the expansive forces generated in small pores (<50 nm) by secondary ettringite formation in saturated conditions ([5,6]). Gypsum formation and leaching of calcium phases are associated with chemical damage that deteriorate the mechanical properties of the matrix (CH and CSH gel). Other types of ESA such as those related to thaumasite formation are described elsewhere [6,7]. Regardless of the damage mechanism associated with the ESA, most standard and recommendations to mitigate the consequences of the attack rely on the specification of sulphate-resisting (SR) cements characterized by a limited C_3A content (generally below 5% by cement weight [6,7]).

Nevertheless, this countermeasure only considers aluminates in the cement, falling short to account for the influence of aluminates coming from other sources, like the accelerators. It also does not account for the higher interconnected porosity induced by the spraying process and the very early exposure to sulphates that could favour the sulphate ingress and the ESA in comparison with conventionally cast matrices.

The lack of specific considerations might be a consequence of the limited knowledge about the impact of the spraying process with accelerators in the durability to ESA. To illustrate it, Table 1 summarises the variables and experimental methods from studies published in the

* Corresponding author.
** Corresponding author.
E-mail addresses: carlos.manuel.herrera@upc.edu (C. Herrera-Mesen), S.Cavalaro@lboro.ac.uk (S.H.P. Cavalaro).

https://doi.org/10.1016/j.cemconcomp.2020.103614
Received 12 August 2019; Received in revised form 26 March 2020; Accepted 30 March 2020
Available online 15 August 2020

Table 1
Recent studies about the ESA in matrices with Portland cement.

			References									This work
			[10]	[11]	[12]	[13]	[14]	[15]	[16]	[17]	[18]	[19]	
Variables	Before exposition (days)		57	57	15	14	14	14	57	28	–	7	7 and 28
	Type of mix	Cast	•		•	•	•	•	•	•	•	•	•
		Spray	•	•									•
	Cement	I	•	•	•								•
		II		•	•	•			•	•	•		•
		SR[a]	×	×	✓	✓	×	×	✓	×	✓	✓	✓
	Accelerators[b]	AF	•	•									•
		AR	•	•									•
Methods	Dimension stability		•	•				•	•		•	•	•
	Velocity of US												•
	Phase composition		•	•	•		•		•	•	•	•	•
	SEM		•	•	•		•	•	•		•		•
	Mechanical tests				•			•		•			•

[a] Sulphate-resisting according to [8,9].
[b] Alkali-free (AF) or alkaline (AR).

Table 2
Phase and chemical compositions of cement.

Phase Composition (%)			Chemical Composition (%)		
	CEM I	CEM II		CEM I	CEM II
C_3S	58.3	51.7	CaO	62.6	62.5
C_2S	11.2	6.7	SiO_2	19.9	17.6
C_4AF	13.4	14.8	Al_2O_3	4.7	4.0
C_3A_c	4.1	2.9	Fe_2O_3	3.3	3.5
C_3A_o	0.6	0.7	SO_3	3.5	3.2
CaO	1.1	1.2	MgO	1.9	1.7
$Ca(OH)_2$	1.7	0.7	K_2O	1.0	0.8
$CaCO_3$	1.9	11.3	TiO_2	0.2	0.2
$CaSO_4{\cdot}2H_2O$	2.1	0.7	P_2O_5	0.1	0.1
$CaSO_4.0.5H_2O$	4.4	5.3	LOI	2.9	6.4
K_2SO_4	–	0.5			
$K_2{\cdot}Ca(SO4)_2{\cdot}H_2O$	1.1	–			
MgO	–	0.6			
$MgCO_3$	–	3.1			
Total	100.0	100.0	Total	100.0	100.0

Table 3
Characteristics of accelerators.

Characteristic	AF060	AF040	AR130	AR080
Solid content	48.0	68.5	43.0	61.9
Al_2O_3 content (%)	13.5	12.0	24.0	16.5
SO_4^{2-} content (%)	21.0	29.0	–	–
Na_2O content (%)	–	–	19.0	19.5
pH at 20 °C	3.1	2.2	12.0	12.5
Al_2O_3/SO_4^{2-} molar ratio	0.6	0.4	–	–
Al_2O_3/Na_2O molar ratio	–	–	1.3	0.8

last 20 years about the ESA in sprayed or cast mixes with and without accelerators.

Notice that only [7,8] evaluate the influence of accelerators on the durability of sprayed mixes exposed to sulphates. Their findings suggest a link between the accelerators and the increase in the degradation induced by the ESA. However, none of these studies evaluates the impact of the age of exposition to the sulphates, assuming a time that might not represent real applications. More importantly, they do not assess the performance of mixes with SR cement, which is essential to elucidate if the recommendation found in codes to mitigate the ESA also suffice for sprayed mixes with the accelerator. This critical gap in knowledge has potentially negative practical repercussions.

The objective of this work is to evaluate how the chemical composition of accelerators and the age of exposition to sulphates affect the degradation mechanism of sprayed mixes with SR cements subjected to ESA. In total, 8 mortar compositions were sprayed in laboratory conditions with 2 SR cement and 4 set accelerators. Cores and prisms were extracted and exposed to a sulphate solution at 7 and 28 days since production for 400 days. Evolution of phases, microstructure and macroscopic behaviour were characterized.

Results complement the limited literature on the behaviour sprayed mixes with accelerator subjected to ESA. Moreover, findings shed light on understanding the ESA consequences in sprayed mixes with SR cement at micro- and macro-structural levels depending on the accelerator type. Observations derived here might guide the selection of materials to enhance the durability of sprayed structures and help steer the definition of more appropriate recommendations in standards to mitigate the ESA in such application.

Table 4
Chemical composition of sprayed mortars.

Name	Composition (mmol/g $_{cement}$)						
	Total SO_4^{-2} in cement	Al in accele.[a]	SO_4^{2-} in acceler.	AFt formed[b]	SO_4^{2-} consumed by AFt formation[C]	SO_4^{-2} left	Final Al/SO_4^{-2}
CI_REF[(d)]	0,44	–	–	–	–	0,44	0.59
CI_AF060_5%	0.44	0.13	0.11	0.07	0.20	0.35	0.73
CI_AF040_5%	0.44	0.12	0.15	0.06	0.18	0.26	0.63
CI_AR130_3%	0.44	0.14	–	0.07	0.21	0.23	1.13
CI_AR080_3%	0.44	0.10	–	0.05	0.15	0.29	0.90
CII_REF[(d)]	0.40	–	–	–	–	0.40	0.44
CII_AF060_5%	0.40	0.13	0.11	0.07	0.20	0.31	0.56
CII_AR080_3%	0.40	0.10	–	0.05	0.15	0.25	0.70

[a] Al corresponds to Al3+ and [Al(OH)4]- in alkali-free and alkaline accelerators, respectively.
[b] AFt phase formed by the accelerator.
[C] Corresponds to the SO_4^{-2} consumed during the formation of the Aft phase.
[d] Not sprayed.

2. Experimental program

2.1. Materials

Mortar mixes contained either Cement I 52.5R (CEM I) or Cement II/A-L 42.5 R (CEM II) with 11.3% of limestone filler by cement weight (bcw). The former is employed in sprayed mixes in Asia and America [2,3], whereas the latter is widely used in Europe. Table 2 summarises the phase and chemical compositions of the cement determined by quantitative XRD and XRF spectrometry, respectively. Both cements comply with the requirements described in [20] and are SR according to [8,9].

A limestone aggregate (>95% $CaCO_3$) with a particle density of 2.32 g/cm^3 was used. In addition, water absorption of the aggregate according to the standard [21] was 5.46%. The particle size distribution of the aggregate rages from 0 mm to 1.25 mm, which is limited by the spraying equipment used in the experimental programme. Distilled water and a superplasticiser based on a polycarboxylate solution (34% solid content) were employed.

To represent the typical types in tunnelling applications, 2 alkali-free accelerators (AF060 and AF040), named because of the Al_2O_3/SO_4^{2-} molar ratio and based on aqueous solutions of aluminium sulphate and 2 alkaline accelerators (AR130 and AR080) named because of the Al_2O_3/Na_2O molar ratio and based on aqueous solutions of sodium aluminate were chosen. Table 3 shows the main characteristics of these accelerators according to the supplier.

2.2. Composition and preparation of mortars

Since the size of the aggregate does not play a key role in the chemical processes involved in the ESA, results obtained here might be taken as a reference of the trend expected for sprayed concrete and mortar [11]. The mixes were produced and tested at the Laboratory of Structures Luis Agulló at Polytechnic University of Catalonia and the Technological Center from the University of Barcelona (CCIT-UB).

Each batch served the production of specimens for all tests of each composition. The batches had 30 kg of cement, an aggregate/cement ratio equal to 1.7 by weight, water/cement (w/c) ratio equal to 0.51 by weight and 1.0% of superplasticiser bcw. The w/c ratio adopted was defined to comply with the pumpability requirements of the spraying equipment. The following contents of accelerator bcw were determined according to Refs. [2] to represent the range typically found in tunnels executed with sprayed materials: 5% and 7% for AF060, 5% for AF040, 3% for AR130 and 3% for AR080.

Table 4 presents the ionic composition of each mix and their corresponding nomenclature that includes the Cement type (CI or CII), accelerator type (REF, AF060, AF040, AR130 and AR080), accelerator dosage in percentage and age of exposition (7 or 28 days), in this order and separated by "_". The final Al/SO_4^{-2} M ratio (Eq. (1)) of the mixtures was calculated by considering the total amount of sulphate remaining after the accelerator reaction. According to Eq. (1) (units in mol), sulphate remaining after accelerator addition (SO_4^{-2} left) corresponds to the sum of the sulphate contents in the cement (SO_4^{-2} in cement) and in the accelerator (SO_4^{-2} in accelerator) minus the sulphate consumed by the aluminium to form ettringite (SO_4^{-2} consumed by AFt formation).

$$\text{Final } \frac{Al}{SO_4^{-2}} = \frac{Al_{cement}}{SO_4^{-2}{}_{cement} + SO_4^{-2}{}_{accelerator} - SO_4^{-2}{}_{consumed\ by\ accelerator}} \quad \text{(Eq 1)}$$

The mixing process was performed in a planetary mixer type 65/2 K-3 with 150 and 40 rpm paddle and planetary rotations, respectively. First, all the cement and 90% of the water were mixed for 240 s. Then, the superplasticizer was added with the remaining water and homogenised for 240 s. Finally, the aggregate was added and mixed for 300 s. After the mixing process, mortars were kept for 1 h at 20 °C until the spraying process. This procedure, also adopted by [3,22,23], intends to reproduce the typical field conditions as concrete must be transported from the batching plant to the jobsite before spraying takes place.

2.3. Spraying process

The wet-mix spraying process is the most commonly used in underground construction around the world [2] and was selected for this

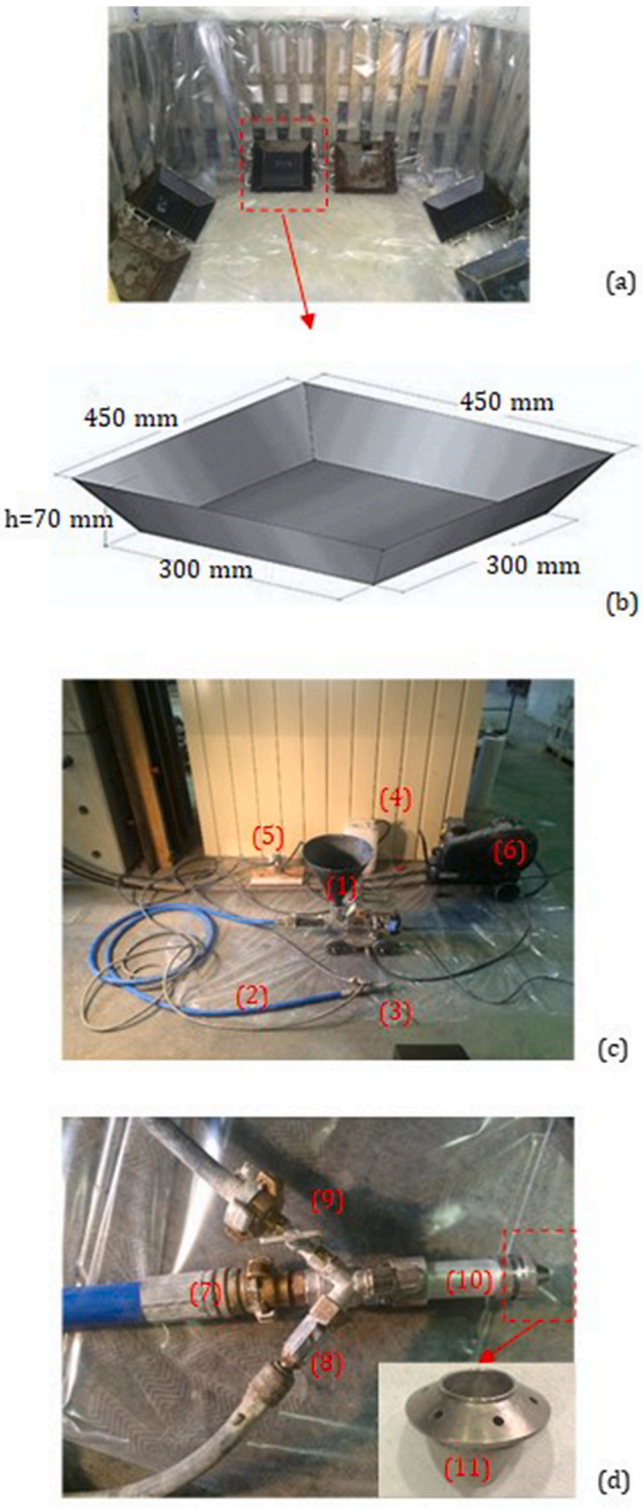

Fig. 1. (a) Arrangement of panels inside the climatic chamber, (b) dimensions of the metallic panels, (c) spraying equipment in laboratory conditions and (d) spray gun.

experimental programme. The spraying happened inside a climatic chamber at 20 °C and 90% relative humidity. The mortar was sprayed in metallic panels forming a 45° angle with the horizontal plane and placed inside the climatic chamber shown in Fig. 1 a. The dimensions (see Fig. 1b) and spraying of the panels were based on [24].

The equipment used to spray the mortars in the laboratory (see Fig. 1c) is a small-scale version of the setup found in previous research [2] and underground construction with concrete. The mortar was pumped by the UP-Pictor screw pump (Fig. 1 c item #1) operating at 6 bar of pressure provided by 3 HP air compressor. The screw pump was chosen for its constant flow and absence of pulsation effect.

The material moved through the hose (Fig. 1 c item #2) and entered the spray gun (Fig. 1 c item #3) through the main entrance (Fig. 1 d item #7). Compressed air (Fig. 1 d item #8) and accelerators (Fig. 1 d item #9) were pre-mixed in a small chamber within the spray gun (Fig. 1 d item #10) and, then, homogenised with the mortar inside the nozzle (Fig. 1 d item #11). The resulting mix exited the nozzle at high speed and was sprayed onto the metallic panels.

The accelerators (Fig. 1 c item #4) were dosed by an air-operated diaphragm pump (Fig. 1 c. item #5) connected to the compressor (Fig. 1 c item #6). This type of pump provided a homogeneous suction for all accelerators tested, regardless of the differences in their viscosity. The flow of accelerators was calculated based on the optimal flow of mortar (5.0 L/min). Once the spraying process ended, the remaining unsprayed mortar was poured in metallic moulds placed horizontally over the ground to produce the reference cast specimens (without spraying and accelerator).

Table 5
Tests performed with cylindrical and prismatic specimens.

Test	Specimen	Number of replicas		Time (days)	Reference
		Sulphate solution	In Water		
Porosity	Cylindrical		3	Prior to sulphate exposure	[26]
Dimensional Variation	Prismatic	6	3	0 to 400	[25]
Visual inspection		6	3	0 to 400	–
Ultrasound Wave Velocity		6	3	0 to 400	[23]
Compressive Strength	Cylindrical	3	3	90	[27]
XRD	Prismatic	1 per age	–	20, 40,150,300	[3,28]
SEM		1 per age	–	400	[29]

2.4. Specimen preparation

All panels remained in the moulds for 24 h, when they were demoulded and placed in a humid chamber (20 °C and 99% relative humidity) for 24 h more. Once the mortar reached enough strength (48 h after production), prismatic and cylindric specimens were extracted and prepared for the tests. Prismatic specimens were saw cut to the dimension 25 × 25 × 250 mm based on the ASTM C490 [25] for assessing the dimensional variation in mortar specimens. Cylindric specimens were drilled using core bits with approximately 25 mm diameter and cut to a length of 25 mm following the methodology in Refs. [24] to ensure the slenderness ratio of 2 [23]. Regions at the inclined edges of the panel and near the mould and outer surfaces were discarded as they are prone to lamination.

After sampling, cores and specimens were subjected to a cleaning process with compressed air and water to eliminate dust or cutting debris filling the pores of the external surface. Finally, dimensions and the presence of damage indicators were checked in all specimens. Those which presented dimensional irregularities (±1 mm) or any signs of damage were discarded.

2.5. Exposure conditions

After the extraction, specimens were submerged in water at 20 °C until the start of sulphate exposure at 7 or 28 days since production, when they were submerged in a sodium sulphate solution with a concentration of 30 g/L and 20 °C. For comparison, reference samples of each composition were submerged in water. The earliest exposure time (7 days) was defined to allow enough time for the preparation of specimens, initial inspection and homogenisation of their saturation degree. The pH of the solutions was measured every 7 days for the first three months and once a month afterwards. The solutions with sulphates were renewed every month or if the pH was above 11.

2.6. Test methods

Table 5 shows the tests performed with cylindrical and prismatic specimens, which include techniques for assessing the macro and microstructural characteristics during the ESA. The start of the exposure to sulphates was considered time 0 for the accelerated ESA tests and the analysis of the results.

An adaptation of the ASTM C490 [25] was used to evaluate the dimensional variation of prismatic specimens. A Digital Demec strain gage measured the change in the distance between 2 stainless steel pins glued 150 mm apart along the biggest size of the specimen. The measurements were taken weekly during the first month and every other week until the end of the test at 400 days. Before assessing the dimensional variation, specimens were subjected to a visual inspection - to

Table 6
Phase structures used in the Rietveld analysis.

Phase	Formula	Crystal System	PDF Codes	ICSD	Ref
Alite	Ca_3SiO_5	Monoclinic	01-070-8632	94,742	[30]
Calcium Aluminate	$Ca_3Al_2O_6$	Cubic	00-038-1429	1841	[31]
Ferrite	Ca_2AlFeO_5	Orthorhombic	01-071-0667	9197	[32]
Gypsum	$CaSO_4 2H_2O$	Monoclinic	00-033-0311	151,692	[33]
Calcite	$CaCO_3$	Rhombohedra	01-083-0577	79,673	[34]
Portlandite	$Ca(OH)_2$	Rhombohedra	01-072-0156	15,741	[35]
Ettringite	$Ca_6Al_2(SO_4)_3·(OH)_{12}·26H_2O$	Hexagonal	00-041-1451	155,395	[36]
Monosulfoaluminate	$Al_2(OH)_{12}·SO_4·6H_2O$	Rhombohedra	–	24,461	[37]
Hemicarboaluminate	$Ca_4Al_2(OH)_{12}·OH·0.5CO_3·4H_2O$	Rhombohedra	00-041-0221	263,124	[38]
Monocarboaluminate	$Ca_4Al_2(OH)_{12}·(CO_3)·5H_2O$	Triclinic	01-087-0493	59,327	[39]
Thenardite	Na_2SO_4	Orthorhombic	01-070-1541	2895	[40]
Dolomite	$CaMg(CO_3)_2$	Rhombohedra	01-075-1761	31,335	[41]
Quartz	SiO_2	Hexagonal	01-083-2465	200,721	[42]
Rutile	TiO_2	Tetragonal	01-089-4202	44,881	[43]

identify cracking, change of colour and spalling - and ultrasound wave velocity test - to indirectly evaluate the matrix deterioration. The equipment Pundit PL-2000 with transducers operating at a frequency of 0.5 MHz in direct transmission was used to measure the ultrasound wave velocity (UWV). The transducers were always placed at the exact half of the specimen to minimise the variability of the results.

To assess the evolution of phase composition over time, X-Ray powder diffraction (XRD) was performed in samples extracted from the prismatic specimens exposed to the sulphate solution. A 2 mm-wide slice was cut from the prismatic specimen at 20, 40, 150 and 300 days. These were crushed and ground to a maximum particle size of 63 μm. The powder obtained was analysed by XRD in a PANalytical X'Pert PRO MPD Alpha1 powder diffractometer in Bragg-Brentano θ/2θ, using CuKα1 (λ = 1.5406 Å) radiation at 45 KV and 40 mA. The powder diagrams were analysed quantitatively by Rietveld refinement using the software X'Pert High Score Plus and the structure models in Table 6. To quantify the amorphous content of the samples, Rutile (99% pure) was added at 20% by sample weight as an internal standard.

Scanning electron microscopy (SEM) was used to analyse the microstructure of samples from the middle region of the prismatic specimen at the end of the attack. These were frozen in liquid nitrogen, vacuum dried during 24 h and coated with carbon. The morphology of phases was analysed in the fracture surfaces, and their chemical composition was assessed by energy dispersive X-ray analysis.

3. Results and discussion

3.1. Porosity characterization before sulphate exposure

Fig. 2 depicts the results of water accessible porosity for all sprayed and poured mixes before immersion in the sulphate solution at 7 or 28 days since production. As expected, a reduction in porosity is observed from 7 to 28 days. Such variation is mainly attributed to the hydration of phases in the cement since the exposition to sulphates had not started yet.

On average, the porosity reduction in the reference compositions (not sprayed and without accelerators) is 2.7 times higher than in sprayed compositions with accelerators. This result confirms findings of previous studies [2,44] and indicates that the incorporation of accelerators compromises the proper consolidation of the sprayed material and the elimination of entrapped air due to the fast setting of the matrix. As described by [45], this may also be explained by the inhibition of alite hydration in accelerated mortars, which limits the amounts of hydration products formed and the filling of pores.

The results obtained are similar to previous publications [2,44]. They suggest that sprayed mixtures have the highest values of porosity

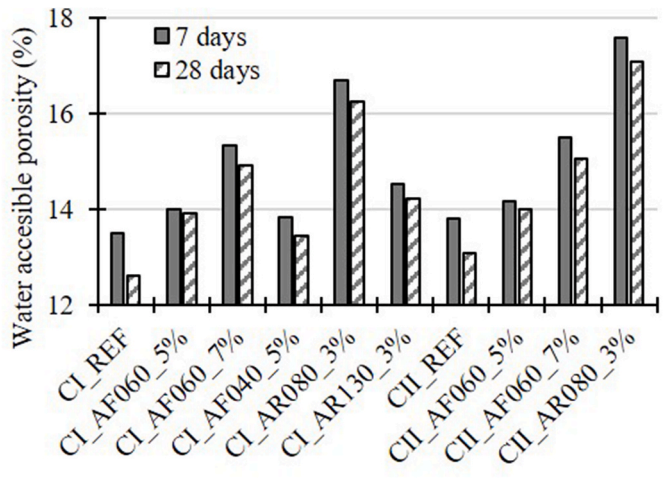

Fig. 2. Water accessible porosity.

at both ages due the incorporation of accelerators, which reduce the setting time of the matrix. Therefore, the matrix does not consolidate properly and does not eliminate the entrapped air, increasing its porosity. The results are directly proportional to the ettringite formation calculated in Table 4, the exceptions are the mixtures with the AR080 accelerator.

Comparing the porosity of CI_AR080_3% (16.24%) and CI_AR130_3% (14.22%), the mixtures that incorporates AR080 presents the lowest ettringite formation and the lowest Al_2O3/Na_2O ratio. One possible explanation is the incorporation of elevated concentrations of sodium, this may lead to a porous matrix [46,47] due to the variation in the composition and density of the C–S–H chains and the AFm phases. The U-phase belongs to the group of hexagonal or pseudo-hexagonal layered structures like the AFm, where sodium is present between the layers increasing the interlayer distance of the crystals [48]. In this case, porosity may be increase by lower density of the C–S–H chains in mixtures with a higher Na^+ content.

In average the reduction in water accessible porosity from 7 to 28 days in the reference mixtures is 5.9%, in the sprayed mixtures this value is 2.2%. As alite hydration is inhibited in accelerated mortars [45], lower amounts of hydration products are formed. Because of that, the filling of pores occurs less intensively, leading to lower reductions in porosity."

3.2. Dimensional variation

Fig. 3a and 3 b show the dimensional variation over time for the specimens with CEM I and CEM II, respectively. The values presented in the graphs are the difference between the average dimensional variation for the composition submerged in the sodium sulphate solution and the average dimensional variation for the same composition submerged in water. This procedure intends to isolate the expansion attributed to the ESA from the expansion that could happen as a result of the hydration of phases in a submerged condition.

The reference cast specimens (CI_REF_28 and CII_REF_28) present negligible dimensional variation caused by sulphate penetration over 400 days of ESA. Such results may be attributed to the low aluminate content of these cement that are considered SR [20] and to the lower porosity of the mixes extracted from cast panels without accelerator. By contrast, the specimens of sprayed mortars with accelerator show expansions ranging from 0.5 to 7 mm/m at 400 days. This may be the result of the higher porosity induced by the spraying process, which could favour sulphate ingress and the additional aluminate content provided by the accelerators that could contribute to the formation of expansive phases.

The mixes with AR accelerators show more significant expansion than the mixes with AF accelerators. Notice that specimens sprayed with AR accelerators present the highest porosity (Fig. 2) amongst all analysed here. The significant expansion of the mix with AR080 accelerator is enough to produce an early failure of the specimens and the interruption of the test. Specimens with AR080 accelerator using CEM I and CEM II exposed to sulphates at 28 days since production failed approximately 120 days after the beginning of accelerated ESA. Specimens with AR accelerator and CEM II exposed to sulphates at 7 days since production withstood even less time in the accelerated ESA, failing only 30 days from the beginning of the test. This suggests that the spraying process with accelerates leads to a significant reduction in the expected durability in comparison with reference cast specimens without accelerators. Such reduction is observed despite using SR cement and is particularly evident in mixes with AR accelerators.

Specimens exposed to sulphates at 7 days since production presented up to 5-times higher expansion than equivalent specimens exposed to sulphates at 28 days since production. These differences appear faster in mixes with AR accelerator than in mixes with AF accelerator. Both outcomes may be related to the more rapid sulphate ingress induced by the larger interconnected porosity at 7 days in comparison with 28 days

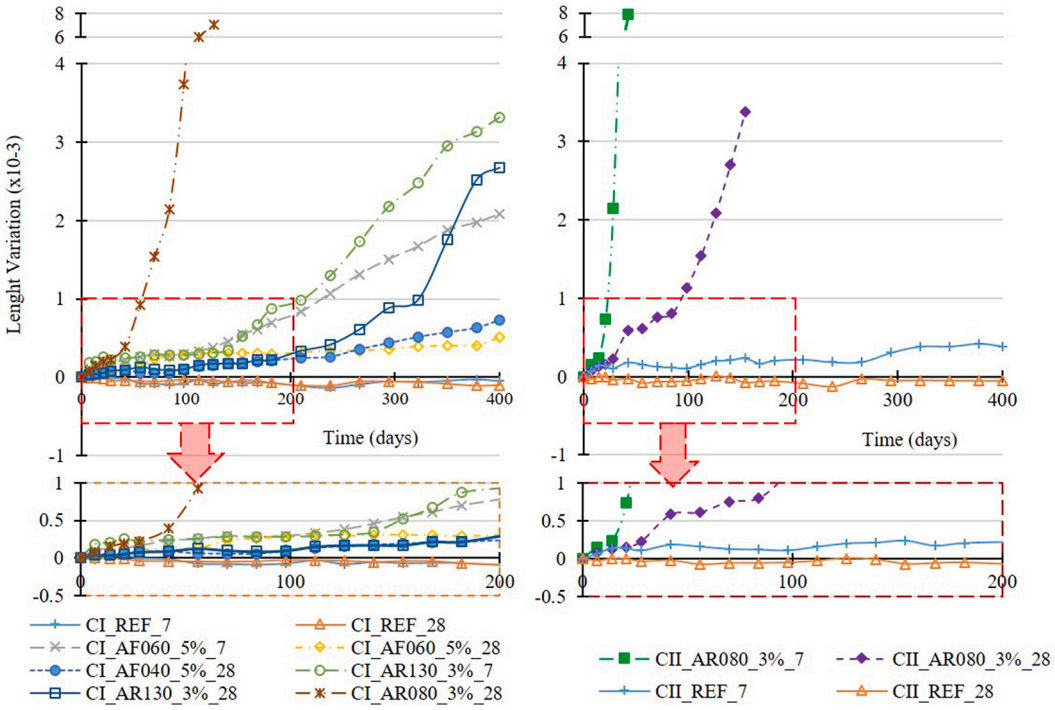

Fig. 3. Dimensional variation in sprayed mortars with (a) CEM I and (b) CEM II.

and in mixes with AR accelerator in comparison with those with AF accelerators.

Skalny et al. [49] suggest an expansion of 0.1% as a safe margin for determining the maximum expansion without significant degradation in mixes under sulphate attack. Crammond [50] recommends that the 0.1% expansion should not be exceeded after 6 months of testing. Although the experimental procedure adopted may affect the results, only cast specimens without accelerators fulfil this requirement, which is consistent with the use of SR cement. Conversely and despite using the same cement, 5 of the mixes sprayed with accelerator show expansions between 2.1 and 8.7 times higher than the limit while the remaining 3 had already failed much before reaching 6 months of testing.

3.3. Visual inspection

Fig. 4 shows images from the visual inspection of specimens at the beginning of the ESA and at the latest time during the test (400 days for those not failing and less for those failing before the end of the test). All cast specimens experience a slight change in their surface colour during the 400 days of sulphate exposure, which may be related to the precipitation of phases (see example in Fig. 4a and 4 b for CI_REF_28 and CII_REF_28, respectively). By contrast, in addition to the change in colour, almost all sprayed specimens with accelerator present cracking, as shown in Fig. 4c to 4j. This confirms that the spraying process with accelerators might reduce the durability in elements exposed to ESA.

The mixes with the accelerator AR080 present the highest degrees of degradation (Fig. 4 f, Fig. 4 i and Fig. 4j), with longitudinal and transversal cracking near the edges and in the central part of the specimens. These results are consistent with the higher expansion measured in sprayed mixes with AR accelerator.

Edge cracking is usually the first visual consequence of the ESA, associated with an intensification of sulphate penetration combined with low material confinement in those regions. Longitudinal and cracking of the cross section are serious failure modes caused by the interaction between the sound core of the specimen and the external layers directly affected by sulphate penetration. Fig. 4 shows that failure in the cross-section happens more often than longitudinal cracking or spalling, which agrees with the findings by [51,52]. These authors stated that the tensile stress generated in the core of specimens with small cross-section due to the expansion of the external layers (related to cross-sectional failure) are more critical than the stress generated in the interface between the damaged and sound regions (related to spalling).

Specimens exposed to sulphates at 7 days show earlier formation of cracks and higher degrees of damage than specimens exposed to sulphates at 28 days. The comparison of specimens with different cement types (Fig. 4a and 4 b or Fig. 4f and 4 i) does not reveal any significant difference, thus suggesting a similar behaviour.

3.4. Ultrasound wave velocity (UWV)

Fig. 5 presents the evolution of the UWV over time for mixes subjected to ESA. Variations in the UWV are caused by changes in the density, elastic modulus and integrity of the specimens. All curves in Fig. 5 show a similar trend characterised by two stages: an increase of the UWV up to a maximum (Stage 1) followed by a reduction of UWV until the end of the test or failure of the specimen (Stage 2).

Stage 1 comprises the early ages of the attack when the phases produced by cement hydration and the ESA contribute to reduce the porosity and the ESA contribute to reduce the porosity and improve the mechanical properties of the mixture cause by the space filling. This effect caused by the precipitation prevails. In Stage 2 - comprehending from maximum UWV onwards - the deposition of expansive phases causes significant micro-cracking that acts like obstacles to the wave propagation. This effect prevails over the potential increase arising from the densification of the matrix.

Table 7 summarises the initial UWV at the start of the exposure to ESA (UWV_0), the variation observed during the test (UWV_{end} - UWV_0), the maximum velocity (UWV_{max}) and the time it occurs (t_{max}), and the maximum variation (UWV_{end} - UWV_{max}). Notice that UWV_{end} refers to the last measurement taken (at 400 days for specimens not failing and at time of failure for others).

From time 0 to the end of the test, cast mixes experience a UWV increase consistent with limited micro-structural damage due to the ESA. Conversely, sprayed mixes with accelerators present mainly

Fig. 4. Visual inspection of the cast and sprayed specimens before and after the accelerated ESA.

negative UWV variations, which indicate significant micro-structural deterioration.

UWV_{max} occurs 2.3 to 6.0 times earlier in sprayed mixes with accelerator than in cast mixes without accelerator. This reveals a quicker onset of the damage, possibly due to a more rapid sulphate ingress promoted by the higher porosity and the capacity to form expansive phases in sprayed mixes with accelerators. After reaching UWV_{max}, cast mixes experience a UWV reduction 14 times smaller than that observed in sprayed mixes with accelerators, which confirms the more intense damage of the latter due to the ESA.

The level of degradation assessed for mixes with AR accelerators is on average 2.5 times higher than that of mixes with AF accelerators. Such results are consistent with the visual inspection and the dimensional variation in Fig. 3. Mixes with Al_2O_3/Na_2O ratio of 0.8 (AR080) present a higher deterioration in a shorter period than the mixes with Al_2O_3/Na_2O ratio of 1.3 (AR130). This suggests that a lower Al_2O_3/Na_2O ratio may affect negatively the durability of accelerated matrices exposed to sulphates. The higher proportion of sodium in relation to aluminates could contribute to the formation of AFm with higher solubility that would react and form ettringite more quickly.

3.5. Compressive strength

Table 8 shows the average compressive strength ($\overline{X}$) at 98 days for the mixes with CEM I and the relative reduction between the mixes exposed to sulphate and equivalent ones in water. All compositions exposed to sulphates show a strength reduction due to the progressive micro-cracking associated with the ESA. The mix CI_REF_28 presents the smallest relative reduction, which reflects the limited damage expected in cast mixes with SR cement.

Relative reductions are marginally higher in sprayed mixes with AF accelerators for the first 98 days of exposition to sulphates, which suggests that the additional damage observed in the UWV and dimensional variation caused by the ESA does not significantly compromise the compressive strength. Conversely, sprayed mixes with AR accelerator showed relative differences 6.6 to 9.6 times higher than those of cast

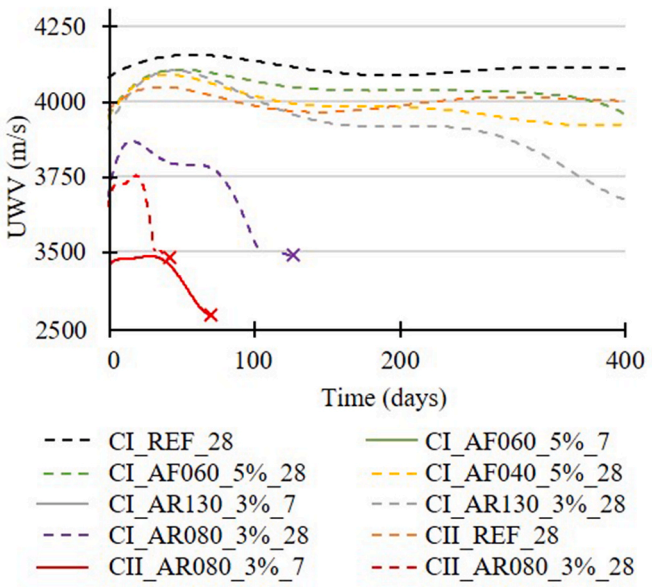

Fig. 5. UWV in mixes subjected to ESA.

Table 7
Parameters obtained from the UWV curves in Fig. 5.

Mortar Sample	UWV_0 (m/s)	UWV_{max} (m/s)	t_{max} (days)	$UWV_{end} - UWV_{max}$ (m/s)	$UWV_{end} - UWV_0$ (m/s)
CI_REF_28	4055.6	4158.9	126	−46.1	57.2
CI_AF060_5%_7	3881.9	4115.1	56	−230.2	3.0
CI_AF060_5%_28	3938.5	4107.1	56	−146.0	22.6
CI_AF040_5%_28	3946.9	4104.7	21	−163.5	−5.7
CI_AR130_3%_7	3826.3	4007.4	42	−474.8	−293.8
CI_AR130_3%_28	3872.8	4107.8	28	−454.2	−219.2
CI_AR080_3%_28	3697.0	3887.8	28	−438.7	−247.9
CII_REF_28	3980.5	4062.7	126	−50.8	31.4
CII_AR080_3%_7	3318.6	3471.4	21	−797.2	−644.4
CII_AR080_3%_28	3651.5	3753.7	21	−338.8	−236.6

Table 8
Compressive strength for mortars with CEM I.

Mix	In water		In Na_2SO_4 solution		Relative reduction
	$\bar{X}$(MPa)	CV (%)	$\bar{X}$(MPa)	CV (%)	(%)
CI_REF_28	38.66	5.48	36.80	11.38	4.83
CI_AF060_5%_7	31.48	26.04	29.15	21.04	7.38
CI_AF060_5%_28	33.32	19.78	31.19	24.07	6.40
CI_AR130_3%_7	31.57	12.96	16.98	23.06	46.24
CI_AR130_3%_28	34.70	23.93	23.69	19.74	31.72

specimens and overall compressive strength reductions of up to 46.24%. The results confirm that the accelerator type influences significantly the compressive strength during the first 98 days of the accelerated ESA.

Sprayed mixes with AF and AR accelerators exposed at 7 days since production present respectively 13.3% and 31.4% higher relative strength reduction in comparison to corresponding ones exposed at 28 days since production. In other words, the sprayed mix with AR accelerator is 2.2 times more sensitive to the age of exposition than equivalent sprayed mix with AF accelerator. The trends observed here are consistent with those identified in previous tests.

3.6. X-ray diffraction

Fig. 6 shows the mass percentage of ettringite (6. a) and gypsum (6. b) formed during the exposition to sulphates. The quantification of AFm was deemed not accurate enough due to the low intensity of the AFm peaks compared to the intensity of calcite peaks from the aggregate (>60% of the composition by weight). Assessment for mixes whose specimens failed before the end of the test were only conducted until the damage led to a free sulphate ingress in the matrix, thus potentially compromising the quantification. The missing results for later times are represented in red with the same magnitude as the last valid quantification.

The amount of ettringite in mixes without accelerator (CI_REF_28 and CII_REF_28) is significantly smaller than in the rest of sprayed mixes throughout the accelerated test. Since accelerators provide an extra source of aluminium to the mortar, a larger amount of AFm phase is expected as hydration progresses [3,22]. Therefore, more ettringite should be quantified in accelerated matrices as AFm phases react with the sulphate ions from the solution, forming secondary ettringite. The secondary ettringite formed is the main responsible for the expansion in Fig. 3 and the degradation found in visual inspections, UWV and compressive strength.

The amount of gypsum (Fig. 6b) is lower than 1% in all mixes except for the ones with AR080 accelerator. The formation of gypsum can be a preliminary stage to the formation of ettringite. However, as mentioned by [20], it is still unknown if the gypsum intervenes in the expansions and deterioration caused by the ESA.

The formation of secondary ettringite is also influenced by the accelerator type. Mortars containing AR accelerators (CI_AR130_3%_28 and CI_AR080_3%_28) present larger amounts of ettringite compared to the equivalent mortars produced with AF accelerators (CI_AF060_5%_28 and CI_AF040_5%_28) at 300 days of ESA. Since the AR accelerators has a higher Al/SO_4^{-2} ratio, larger amounts of AFm phases are formed, leading to a higher quantity of secondary ettringite during the ESA.

The higher amount of ettringite in mortars containing AR accelerators is also influenced by the addition of sodium to the mix. The AFm formed in the presence of high sodium concentration is in a U-phase [22,28]. The U-phase is a mineral observed for first time by Dosch and zur Strassen [53]. In their study they found that a new phase was formed and the plausible composition was established as $4CaO{\cdot}0.9Al_2O_3{\cdot}l.lSO{\cdot}0.5Na_2O{\cdot}16H_2O$, and it belongs to the group of hexagonal or pseudo-hexagonal layered structures like the AFm, where sodium is present between the layers increasing the interlayer distance of the crystals [48].

The cast mixes with CEM I present higher content of ettringite than equivalent mixes with CEM II. This is consistent with the higher C_3A content in the CEM I (4.7% bcw) in comparison with CEM II (3.6% bcw), which should be proportional to the potential to form ettringite. The same trend is not as clear in sprayed mixes due to the interaction with compounds provided by the accelerators and the early damage experienced by specimens.

Results at 300 days reveal that mixes exposed to sulphates at 7 days since production have approximately 1.33 times more ettringite than equivalent mixes exposed to sulphates at 28 days since production. The larger ettringite content is also related to the higher connected porosity of mixes exposed at earlier ages, which favours the sulphate ingress and the consequent formation of ettringite. As hydration progresses, the porosity is reduced, limiting the diffusion of sulphates in the matrix. The influence of this variable is particularly evident in mixes with AR080 accelerator whose specimens exposed at 7 days since production have twice as much ettringite as specimens exposed at 28 days. This is possibly one of the reasons for the earlier failure of specimens exposed to

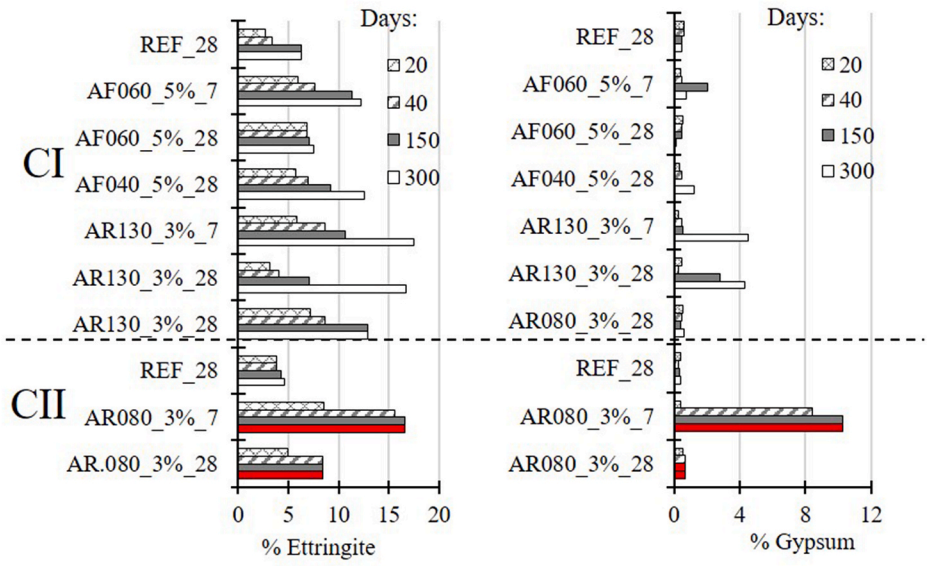

Fig. 6. Phases formed in the mixes: (a) Ettringite and (b) Gypsum.

sulphates at 7 days in comparison with those exposed at 28 days since production.

3.7. Scanning electron microscopy

Mortar compositions CI_REF_28, CI_AF060_3%_28, CI_AR130_3%_28 and CI_AR080_3%_28 exposed to sulphates were evaluated through SEM at 400 days. Fig. 7 shows the results for the cast mix CI_REF_28 without accelerator. The regions analysed by EDS are indicated by a white circle in the image. Results obtained in the EDS spectra are represented as the atomic relative intensities of each element, placed above each image. These intensities are important to identify the relative relation between each other and correlate with the chemical composition of the phases analysed. The peaks considered to measure the intensity of Ca, Si, S and Al correspond to the energies of 3.73, 1.78, 2.33 and 1.52 keV, respectively. Normally, the ultimate phase of the aluminium hydration is monosulfoaluminate (Al/S = 2 and C-A-H hydrates (Al/S $\geq$ 0.66). Al/S ratio values between 0.33 and 0.66 indicate the possible presence of a secondary product like ettringite in the pores [3,22,45].

Fig. 7 a shows a pore filled with plate-like crystals. The Al/Ca, Si/Ca, and Al/S atomic ratios are respectively equal to 0.24, 0.16 and 0.72, indicating a potential presence of C–S–H, AFt and AFm phases. Further approximation inside the pore reveals needle-like crystals measuring 10 μm in length characterised by an Al/S atomic ratio of 0.63, indicating the presence of ettringite (see Fig. 7b). Ettringite in this case seems to appear with the AFm phase (Al/S $\geq$ 0.66) indicating that secondary ettringite is barely formed due to the low C_3A content in the cement. Normally, it is expected to find ettringite in earlier stages of hydration. However, these samples are 400 days old and the main hydrate formed by C_3A hydration are AFm phases, which present Al/S ratios higher than 2. The results are in line with the low ettringite formation detected in XRD analyses of the mix (see Fig. 6). Sodium was not identified in the EDS of the sample.

Fig. 8 shows the SEM images and the EDS of the sprayed mix CI_AF060_5%_28. The EDS spectrum In Fig. 8 a shows Al/Ca, Si/Ca and Al/S atomic ratios respective equal to 0.11, 0.19 and 1.1, indicating presence of C–S–H and AFm phases. The main sulfoaluminate phase found was AFm, which can be related to the introduction of sulphates ions by the accelerator.

Fig. 8 b shows a pore filled with 20 μm-long needle-like formation with an Al/S atomic ratio of 0.30, indicating a combination of AFt phase and sulphates. This is consistent with the XRD results that show increasing contents of ettringite in mixes with AF accelerator in comparison with those without accelerator. Once more, sodium was not found in the matrix or the pores.

Fig. 9 shows SEM images and the EDS analysis of the mix CI_AR130_3%_28. Fig. 9 a reveal Al/Ca, Si/Ca and Al/S atomic ratios that suggest the presence of ettringite and C–S–H. In this case, sodium is

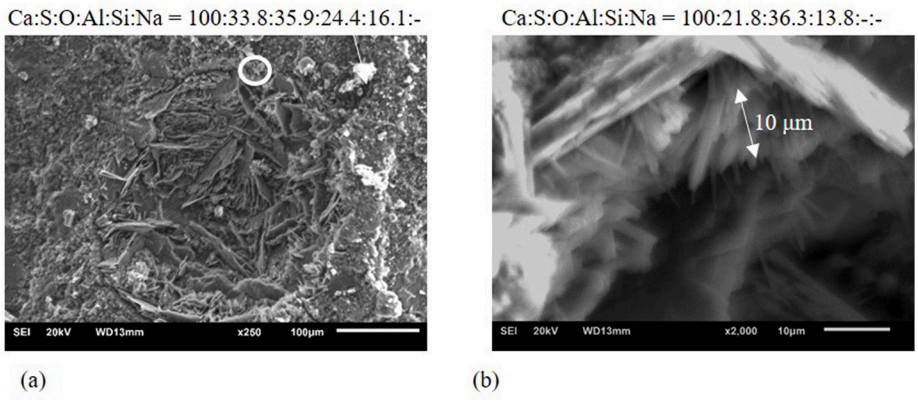

Fig. 7. SEM images and EDS analysis of pore (a) and detail of ettringite formation (b) in CI_REF_28.

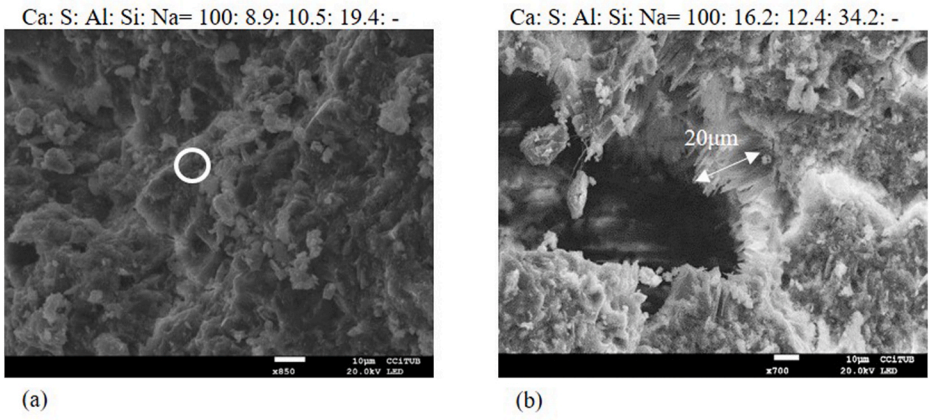

Fig. 8. SEM image and EDS analysis of the matrix (a) and ettringite formation (b) in CI_AF060_5%_28.

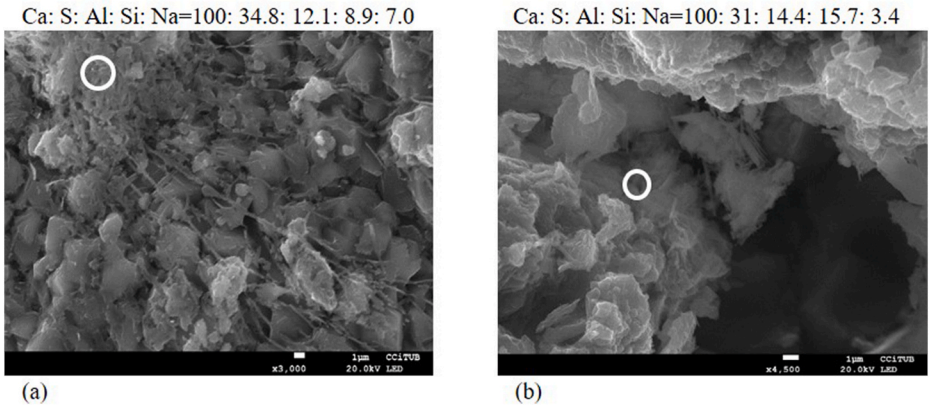

Fig. 9. SEM image and EDS analysis of the matrix (a) and ettringite (b) in CI_AR130_3%_28.

found in EDS results of the sample. The sodium could come from the alkaline accelerator and the Na_2SO_4 diluted in water. Since the sodium was only found in the mixes with the AR accelerator, the most likely source is deemed the accelerator that incorporates Na^+ and Al $[(OH)_4]^-$ ions into the matrix during hydration [3]. Depending on the Na^+ concentration, phases with sodium, calcium and aluminate may be formed.

The presence of sodium may lead to a more porous matrix [46,47] due to variation in the composition of C–S–H and AFm phases. In Fig. 9 a, sodium is found in the C–S–H composition, which changes to a system with lower density due to the lower Ca–Si/(Si + Al) ratio compared to alkali-free systems [46,47]. AFm phases were not found in Fig. 9, probably due to the enhanced solubility of these phases in the presence of sodium. Fig. 9 b shows the inside of a pore characterised by an Al/S ratio equal to 0.46 that is consistent with ettringite in the presence of sulphates.

Fig. 10 shows the SEM images and the EDS of the mix CI_AR080_3%_28. According to the EDS results in Fig. 10 a, Al/Ca, Si/Ca, and Al/S atomic ratios respectively of 0.07, 0.15 and 0.38 indicate a possible presence of C–S–H and AFt phases. Sodium is also found with a Na/Ca atomic ratio equal to 0.23, which is higher than in the mix with AR130

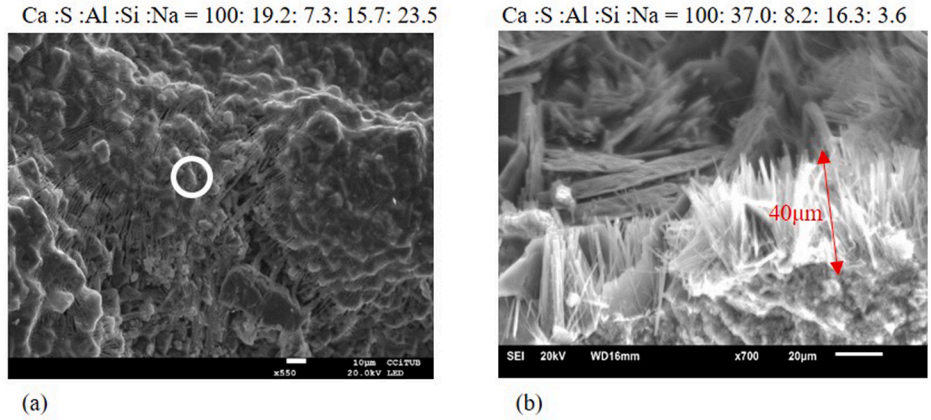

Fig. 10. SEM image and EDS analysis of (a) detail of the C–S–H and (b) Ettringite formation in CI_AR080_3%_28.

(0.07). Sodium seems to remain in the C–S–H, which explains the higher porosity found in the mixes with accelerator AR080. Fig. 10 b shows the formation of 40 μm-long needle-shaped crystals with Al/S atomic ratio equal to 0.22, indicating a typical ettringite formation with a high content of sulphates. These are the longest and more abundant ettringite needles found across all specimens analysed, thus justifying the XRD results and the damage observed in sprayed mixes with AR080.

4. Influence of theoretical Al/SO_4^{-2} of the mix with accelerator

Fig. 11 shows the relationship between the theoretical Al/SO_4^{-2} of the mix with accelerator summarised in Table 4 (x-axis of all graphs) and the main results obtained in the experimental programme (y-axis). Only results of mixes exposed to sulphates 28 days since production are depicted in Fig. 11 to ensure the comparison under nearly identical conditions. The reduction of compressive strength and porosity were assessed at 90 days of sulphate exposure and just before sulphate exposure, respectively. Other results correspond to approximately 300 days of accelerated ESA.

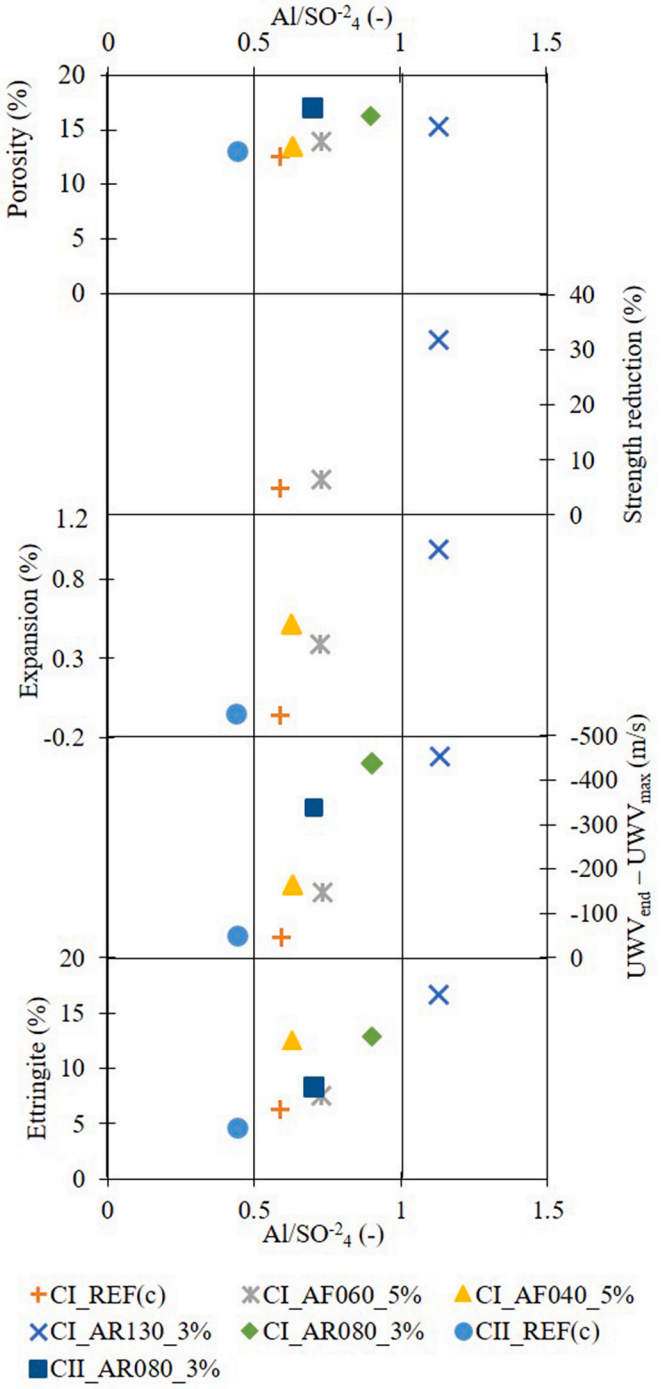

Fig. 11. Relationship between the theoretical Al/SO_4^{-2} of the mix with accelerator and the ettringite formation, maximum ultrasound variation, linear expansion, strength reduction and porosity (Table A.1).

A similar linear trend is observed for the ettringite formation, the maximum ultrasound variation, the linear expansion and the reduction of compressive strength (notice that results for only 3 mixes are available for the latter). This confirms that the increase of the theoretical Al/SO_4^{-2} of the mix with the accelerator is related to the potential ettringite formation and the consequent magnitude of micro- and macro-structural changes induced by the ESA. A less clear trend was observed with the porosity, which is influenced by other aspects related to the production process that might have eclipsed the effect of the Al/SO_4^{-2}.

5. Conclusions

The following conclusions are derived from the study conducted here.

- Sprayed mixes with accelerator showed more ettringite, larger ettringite crystals and several times larger linear expansion than equivalent cast mixes without accelerator. This led to more damage at the micro- and macro-structural levels observed in the ultrasound results, visual inspection and mechanical tests results.
- The spraying process increases the interconnected porosity and favours the sulphate ingress. The inclusion of set accelerators provides an additional amount of aluminate phases that may react with sulphates in the ESA and contribute to the development of expansion and damages. Both factors seem the main responsible for the higher vulnerability to the ESA of sprayed mixes with accelerator in comparison with equivalent cast mixes without accelerator.
- Alkaline accelerators triggered higher ettringite formation, expansion and deterioration than alkali-free accelerators. The absence of sulphates in alkaline accelerators leads to larger amounts of AFm phases (main source of secondary ettringite). Notice that ettringite was consistently found within the gel in sprayed mixes with alkaline accelerators tested here. Expansive products formed at these locations are more likely to generate damage due to the low capacity of the gel to accommodate the expansions
- The results suggest that the age of sulphate exposure plays a major role in the durability of sprayed specimens to the ESA. Specimens exposed at 7 days since production had significantly higher deterioration and expansion than those exposed at 28 days since production. As most sprayed structures are exposed to sulphates immediately after spraying, the accelerated ESA on specimens should be performed at earlier ages to obtain more realistic predictions for such applications.
- Despite using SR cement in all mixes, sprayed specimens presented severe and early signs of damage, which was not found in any of the reference cast specimens without accelerator. While both cast mixes without accelerator experienced expansion below the limit considered safe according to the literature [49,50]. This reveals that the use of SR cement in sprayed mixes with accelerators is not enough measure to mitigate the consequences of the ESA.

Based on these findings, the following practical recommendations are proposed to reduce the negative consequences of ESA in elements exposed to sulphates and constructed with sprayed mixes with accelerators.

- The common practice found in guidelines and adopted in projects that rely mainly on the use of SR cement should be revisited.

Limitations should be defined for the total content of potentially expansive aluminates (cement + accelerator) per volume of concrete and the Al/SO_4^{-2}.

- In the absence of such recommendations, specific experimental tests should be conducted to assess the impact of spraying with accelerators on the durability of mixes subjected to ESA.
- Alkali-free accelerators should be the preferred choice in applications under risk of ESA. If alkali-rich accelerators must be used, those with lower sodium content should be chosen.

Declaration of competing interest

The authors declare that they have no known competing financial interests or personal relationships that could have appeared to influence the work reported in this paper.

Acknowledgements

The first author thanks the CONICIT (Consejo Nacional para Investigaciones Científicas y Tecnológicas, process FI-108B-14) of Costa Rica for the scholarship. The second author thanks FAPESP (Fundação de Amparo à Pesquisa do Estado de São Paulo, process 2017/00125-9) for the scholarship. This research was possible due to the projects BIA2016-78740-R (MAPPU) and RTC-2015-3185-4 (MAPMIT), co-funded by the Ministerio de Economía y Competitividad of Spain in the Call Retos-Colaboración 2015 and by the European Union through FEDER funds under the objective of promoting the technological development, innovation and high quality research. Special thanks for the technical and financial support to Industrias Químicas del Ebro, to Centro para el Desarrollo Industrial (CDTi) and to the Ministerio de Economía y Competitividad, all of them in the context of the project IDI-20130248.

Appendix A. Appendix

Results obtained by periodic measures of length variation are shown in Table A.3. The values presented in the tables are the difference between the average dimensional variation for the composition submerged in the sodium sulphate solution and the average dimensional variation for the same composition submerged in water.

Table A.1
Length Variation (x 10^{-3}) of the mixtures from 0 to 98 days.

Mixtures	Time (days)									
	0	7	14	21	28	42	56	70	84	98
CI_REF_7	0	−0.021	0.019	0.033	−0.006	−0.017	−0.078	−0.082	−0.090	−0.077
CI_REF_28	0	−0.002	−0.007	−0.016	−0.041	−0.045	−0.050	−0.054	−0.047	−0.031
CI_AF060_5%_7	0	0.101	0.121	0.131	0.163	0.226	0.254	0.292	0.275	0.292
CI_AF060_5%_28	0	0.016	0.042	0.083	0.108	0.121	0.130	0.233	0.260	0.280
CI_AF040_5%_28	0	0.042	0.055	0.061	0.080	0.085	0.057	0.056	0.052	0.100
CI_AR130_3%_7	0	0.182	0.201	0.254	0.219	0.241	0.253	0.283	0.284	0.282
CI_AR130_3%_28	0	0.034	0.036	0.052	0.079	0.090	0.126	0.099	0.085	0.096
CI_AR080_3%_28	0	0.081	0.148	0.195	0.221	0.396	0.923	1.534	2.137	3.738
CII_AR080_3%_7	0	0.153	0.232	0.736	2.144	7.846	–	–	–	–
CII_AR080_3%_28	0	0.069	0.126	0.155	0.228	0.585	0.613	0.757	0.800	1.127
CII_REF_7	0	0.065	0.140	0.138	0.107	0.182	0.158	0.127	0.119	0.109
CII_REF_28	0	−0.032	−0.002	−0.005	−0.041	−0.028	−0.081	−0.064	−0.063	−0.056

Table A.2
Length Variation (x 10^{-3}) of the mixtures from 112 to 294 days.

Mixtures	Time (days)									
	112	126	140	154	168	182	210	238	266	294
CI_REF_7	−0.035	−0.082	−0.057	−0.071	−0.067	−0.071	−0.109	−0.133	−0.088	−0.052
CI_REF_28	−0.036	−0.040	−0.058	−0.043	−0.045	−0.073	−0.104	−0.107	−0.055	−0.056
CI_AF060_5%_7	0.330	0.379	0.457	0.544	0.612	0.698	0.834	1.071	1.314	1.507
CI_AF060_5%_28	0.314	0.293	0.307	0.310	0.301	0.291	0.312	0.334	0.334	0.355
CI_AF040_5%_28	0.134	0.152	0.173	0.191	0.201	0.213	0.242	0.259	0.357	0.435
CI_AR130_3%_7	0.289	0.310	0.341	0.522	0.667	0.872	0.978	1.294	1.726	2.180
CI_AR130_3%_28	0.151	0.167	0.171	0.171	0.217	0.217	0.333	0.413	0.607	0.881
CI_AR080_3%_28	6.001	7.101	–	–	–	–	–	–	–	–
CII_AR080_3%_7	–	–	–	–	–	–	–	–	–	–
CII_AR080_3%_28	1.541	2.082	2.704	3.380	–	–	–	–	–	–
CII_REF_7	0.157	0.200	0.211	0.236	0.170	0.204	0.219	0.185	0.188	0.308
CII_REF_28	−0.032	0.004	−0.016	−0.075	−0.064	−0.057	−0.087	−0.124	−0.032	−0.050

Table A.3
Length Variation (x 10^{-3}) of the mixtures from 294 to 400 days.

Mixtures	Time (days)			
	322	350	378	400
CI_REF_7	−0.061	−0.043	−0.026	−0.049
CI_REF_28	−0.062	−0.084	−0.107	−0.101
CI_AF060_5%_7	1.670	1.872	1.977	2.081
CI_AF060_5%_28	0.390	0.398	0.405	0.507
CI_AF040_5%_28	0.515	0.574	0.633	0.730
CI_AR130_3%_7	2.475	2.954	3.136	3.317
CI_AR130_3%_28	0.985	1.752	2.519	2.674
CI_AR080_3%_28	–	–	–	–
CII_AR080_3%_7	–	–	–	–
CII_AR080_3%_28	–	–	–	–
CII_REF_7	0.385	0.385	0.421	0.387
CII_REF_28	−0.048	−0.051	−0.054	0.171

References

[1] T. Garcia, L. Agulló, A. Aguado, J. Rodríguez-Barboza, Mix design procedure for shotcrete (In Spanish), Hormigón y Acero nº 220 (2001) 43–56.
[2] I. Galobardes Reyes, Characterization and Control of Wet-Mix Sprayed Concrete with Accelerators (Ph.D Thesis), Polytechnic University of Catalunya, 2013.
[3] R.P. Salvador, S.H. Cavalaro, I. Segura, A.D. Figueiredo, J. Pérez, Early age hydration of cement pastes with alkaline and alkali-free accelerators for sprayed concrete, Construct. Build. Mater. 111 (2016) 386–398, https://doi.org/10.1016/j.conbuildmat.2016.02.101.
[4] J. Ortiz, A. Aguado, L. Agulló, T. García, Influence of environmental temperatures on the concrete compressive strength: simulation of hot and cold weather conditions, Cement Concr. Res. 35 (2005) 1970–1979, https://doi.org/10.1016/j.cemconres.2005.01.004.
[5] F.R. Steindl, A. Baldermann, I. Galan, M. Sakoparnig, L. Briendl, M. Dietzel, F. Mittermayr, Chemical resistance of eco-concrete – experimental approach on Ca-leaching and sulphate attack, Construct. Build. Mater. 223 (2019) 55–68, https://doi.org/10.1016/j.conbuildmat.2019.06.189.
[6] F. Mittermayr, A. Baldermann, C. Kurta, T. Rinder, D. Klammer, A. Leis, J. Tritthart, M. Dietzel, Evaporation - a key mechanism for the thaumasite form of sulfate attack, Cement Concr. Res. 49 (2013) 55–64, https://doi.org/10.1016/j.cemconres.2013.03.003.
[7] R. Salvador, D. Rambo, R. Bueno, S. Lima, A. Figueiredo, Influence of accelerator type and dosage on the durability of wet-mixed sprayed concrete against external sulfate attack, Construct. Build. Mater. 239 (2019), 117883, https://doi.org/10.1016/j.conbuildmat.2019.117883.
[8] ASTM C150-07, standard specification for Portland cement, Annu. Book ASTM Stand. 552 (2007).
[9] AENOR, UNE EN 197-1 2011 Composition, Specifications and Conformity Criteria for Common Cements, 2009, pp. 9–11.
[10] C. Paglia, F. Wombacher, H. Böhni, M. Sommer, An evaluation of the sulfate resistance of cementitious material accelerated with alkali-free and alkaline admixtures: laboratory vs. field, Cement Concr. Res. 32 (2002) 665–671, https://doi.org/10.1016/S0008-8846(01)00739-6.
[11] C. Paglia, F. Wombacher, H. Böhni, The influence of alkali-free and alkaline shotcrete accelerators within cement systems: influence of the temperature on the sulfate attack mechanisms and damage, Cement Concr. Res. 33 (2003) 387–395, https://doi.org/10.1016/S0008-8846(02)00967-5.
[12] B. Rasheeduzzafar, S.N. Abduljauwad, Magnesium-Sodium sulfate attack in plain and blended cements, Mater. Civ. Eng. 6 (1994) 201–222.
[13] O.S. Baghabra Al-Amoudi, Attack on plain and blended cements exposed to aggressive sulfate environments, Cement Concr. Compos. 24 (2002) 305–316, https://doi.org/10.1016/S0958-9465(01)00082-8.
[14] F. Bellmann, B. Möser, J. Stark, Influence of sulfate solution concentration on the formation of gypsum in sulfate resistance test specimen, Cement Concr. Res. 36 (2006) 358–363, https://doi.org/10.1016/j.cemconres.2005.04.006.
[15] N.N. Naik, A.C. Jupe, S.R. Stock, A.P. Wilkinson, P.L. Lee, K.E. Kurtis, Sulfate attack monitored by microCT and EDXRD: influence of cement type, water-to-cement ratio, and aggregate, Cement Concr. Res. 36 (2006) 144–159, https://doi.org/10.1016/j.cemconres.2005.06.004.
[16] T. Schmidt, Sulfate Attack and the Role of Internal Carbonate on the formatIon of Thaumasite, École Polytechnique Fédérale De Lausanne, 2007.
[17] Y. Senhadji, M. Mouli, H. Khelafi, A.S. Benosman, Sulfate attack of Algerian cement-based material with crushed limestone filler cured at different temperatures, Turk. J. Eng. Environ. Sci. 34 (2010) 131–143, https://doi.org/10.3906/muh-1003-104.
[18] E.F. Irassar, V.L. Bonavetti, M.A. Trezza, M.A. González, Thaumasite formation in limestone filler cements exposed to sodium sulphate solution at 20°C, Cement Concr. Compos. 27 (2005) 77–84, https://doi.org/10.1016/j.cemconcomp.2003.10.003.
[19] D. Torréns-Martín, L. Fernández-Carrasco, Effect of sulfate content on cement mixtures, Construct. Build. Mater. 48 (2013) 144–150, https://doi.org/10.1016/j.conbuildmat.2013.05.106.
[20] A. Neville, The confused world of sulfate attack on concrete, Cement Concr. Res. 34 (2004) 1275–1296, https://doi.org/10.1016/j.cemconres.2004.04.004.
[21] ASTM C 128 -07a : density, relative density (specific gravity), and absorption of fine aggregate, ASTM Int. (2007) 1–7.
[22] C. Herrera-Mesen, R.P. Salvador, S.H.P. Cavalaro, A. Aguado, Effect of gypsum content in sprayed cementitious matrices: early age hydration and mechanical properties, Cement Concr. Compos. 95 (2019) 81–91, https://doi.org/10.1016/j.cemconcomp.2018.10.015.
[23] R.P. Salvador, S.H. Cavalaro, I. Segura, M.G. Hernandez, J. Ranz, A.D. de Figueiredo, Relation between ultrasound measurements and phase evolution in accelerated cementitious matrices, Mater. Des. 113 (2017) 341–352, https://doi.org/10.1016/j.matdes.2016.10.022.
[24] AENOR, UNE-EN 14488-1 Ensayos de hormigón proyectado parte 1: toma de muestra de hormigón fresco y endurecido, 2006.
[25] ASTM, ASTM: C490 standard practice for use of apparatus for the determination of length change of hardened cement paste , mortar , and concrete 1, ASTM Int. (2008) 1–5.
[26] ASTM, ASTM C642 standard test method for density, absorption, and voids in hardened concrete, ASTM Int. (2006) 1–3.
[27] ASTM, ASTM C39 standard test method for compressive strength of cylindrical concrete specimens 1, ASTM Int. (2008) 1–7, i.
[28] R.P. Salvador, S.H.P. Cavalaro, M. Cano, A.D. Figueiredo, Influence of spraying on the early hydration of accelerated cement pastes, Cement Concr. Res. 88 (2016) 7–19, https://doi.org/10.1016/j.cemconres.2016.06.005.
[29] K. Scrivener, R. Snellings, B. Lothenbach, A Practical Guide to Microstructural Analysis of Cementitious Materials, Taylor & Francis Group, LLC, Florida, 2016.
[30] M.A.G. de la Torre, A.G. Bruque, S. Campo, J. Aranda, The superstructure of C_3S from synchrotron and neutron powder diffraction and its role in quantitative phase analyses, Cement Concr. Res. 32 (2002) 1347–1356.
[31] J.W. Mondal, P. Jeffery, The crystal structure of tricalcium aluminate, $Ca_3Al_2O_6$, Acta Crystallogr. B 31 (1975), 689 697.
[32] S. Colville, A.A. Geller, The crystal structure of brownmillerite, Ca_2FeAlO_5, Acta Crystallogr. B 27 (1971) 2311–2315.
[33] J.J. Chen, J.J. Thomas, H.F.W. Taylor, H.M. Jennings, Solubility and structure of calcium silicate hydrate, Cement Concr. Res. 34 (2004) 1499–1519, https://doi.org/10.1016/j.cemconres.2004.04.034.
[34] R. Wartchow, Learnt profile -Methode(LP) fuer Calcit und Vergleich mit der “Background peak background”-Methode (BPB), Zeitschrift Fuer Krist 186 (1989) 300–302.
[35] H.E. Petch, The hydrogen positions in portlandite, $Ca(OH)_2$, as indicated by the electron distribution, Acta Crystallogr. 14 (1961) 950–957.
[36] J. Goetz-Neunhoeffer, F. Neubauer, Refined ettringite ($Ca_6Al_2(SO_4)\cdot3(OH)_{12}\cdot26$ (H2O) structure for quantitative X-ray diffraction analysis, Powder Diffr. (2006) 4–11.
[37] R. Allmann, Die Doppelschichtstruktur der plaettchenfoermigen Calcium-Aluminium-H Salze am Beispiel des $(CaO)_3\cdot Al_2O_3\cdot CaSO_4\cdot(H_2O)_{12}$, Neues Jahrb. Fuer Mineral. Monatshefte. (1968) 140–144.
[38] H. Runcevski, T. Dinnebier, R.E. Magdysyuk, O.V. Poellmann, Crystal structures of calcium hemicarboaluminate and carbonated calcium hemicarboaluminate from synchrotron powder diffraction data, Acta Crystallogr. Sect. B Struct. Sci. 68 (2012) 493–500.
[39] O. Francois, M. Renaudin, G. Evrard, A cementitious compound with composition $3CaO\cdot Al_2O_3\cdot CaCO_3\cdot 11H_2O$, Acta Crystallogr. Sect. C Cryst. Struct. Commun. 54 (1998) 1214–1217.
[40] A.G. Nord, Refinement of the crystal structure of thenardite, Na_2SO_4 (V), Acta Chem. Scand. 27 (1973) 814–822.
[41] G. Effenberger, H. Kirfel, A. Will, Untersuchungen zur Elektronendichteverteilung im Dolomit $CaMg(CO_3)_2$, Tschermaks Mineral. Und Petrogr, Mitteilungen 31 (1983) 151–164.
[42] J.D. Jorgensen, Compression mechanisms in alpha-quartz structures -SiO_2 and GeO_2, J. Appl. Phys. 49 (1978) 5473–5478.
[43] K. Cromer, D.T. Herrington, The structures of anatase and rutile, J. Am. Chem. Soc. 77 (1955) 4708–4709.

[44] R.P. Salvador, S.H. Cavalaro, R. Monte, A.D. De, Relation between chemical processes and mechanical properties of sprayed cementitious matrices containing accelerators, Cement Concr. Compos. 79 (2017) 1–40, https://doi.org/10.1016/j.cemconcomp.2017.02.002.
[45] R.P. Salvador, S.H. Cavalaro, M. Cincotto, A.D. Figueiredo, Parameters controlling early age hydration of cement pastes containing accelerators for sprayed concrete, Cement Concr. Res. J. 89 (2016) 230–248, 10.1016.
[46] B.M. Gassó, Impact of Alkali Salts on the Kinetics and Microstructural Development of Cementitious Systems, École Polytechnique Fédérale de Lausanne, 2015.
[47] A. Kumar, Modelling Hydration Kinetics of Cementitous Systems, Ecole Polytechnique Fédérale de Lausanne, 2012.
[48] G. Li, P. Le Bescop, M. Moranville, The U-Phase formation in cement-based systems containing high amounts of Na_2SO_4, Cement Concr. Res. 26 (1996) 27–33.
[49] J. Skalny, J. Marchand, I. Odler, Sulfate Attack on Concrete, Spon Press, 2002.
[50] N. Crammond, Examination of mortar bars containing varying percentages of coarsely crystalline gypsum as aggregate, Cement Concr. Res. 14 (1984) 225–230.
[51] T. Ikumi, S.H. Cavalaro, I. Segura, C. Goodier, S. Austin, Simplified analytical assessment of damaged induced by the external sulphate attack in concrete piles, in: High Tech Concr. Where Technol. Eng. Meet - Proc. 2017 Fib Symp, Springer International Publishing, Cham, 2017, pp. 2282–2289, https://doi.org/10.1007/978-3-319-59471-2_260.
[52] T. Ikumi, S.H.P. Cavalaro, I. Segura, A. Aguado, Alternative methodology to consider damage and expansions in external sulfate attack modeling, Cement Concr. Res. 63 (2014) 105–116, https://doi.org/10.1016/j.cemconres.2014.05.011.
[53] W. Dosch, H. zur Strassen, An alkali-containg calcium aluminate sulfate hydrate, Zement-Kalk-Gips 20 (1967) 392–401, 392.